Modeling and Analysis of Thermal Characteristics of Magnetic Coupler for Wireless Electric Vehicle Charging System

CE LIANG[1], GUANG YANG[2], FENG YUAN[1], XIAOHUA HUANG[3], YING SUN[2], JIN LI[4], AND KAI SONG[2], (Senior Member, IEEE)

[1]School of Instrument Science and Engineering, Harbin Institute of Technology, Harbin 150000, China
[2]School of Electrical Engineering and Automation, Harbin Institute of Technology, Harbin 150000, China
[3]Electrical Engineering and New Material Department, China Electric Power Research Institute, Beijing 100192, China
[4]State Grid Hebei Electric Power Supply Company Ltd., Xiong'an New Area Power Supply Company, Baoding 071000, China

Corresponding author: Kai Song (kaisong@hit.edu.cn)

ABSTRACT The operating temperature of the magnetic coupler in wireless power transfer (WPT) systems for electric vehicles (EVs) determines the system reliability and service life. This paper studies the modeling and analysis of temperature characteristics of a general magnetic coupler. Firstly, a thermal circuit model is established to show the heat transfer of the magnetic coupler in the air. Secondly, the heating mechanism of the coil, core and aluminum (Al) shield plate is studied. The thermal power of each component is calculated, and the temperature distribution is qualitatively given based on the proposed thermal circuit model. Then, the temperature distribution of each component is simulated, and the results are consistent with the theoretical analysis. Finally, a 6.6 kW WPT prototype is set up, and the temperature of each component is measured after 30 minutes of operation. The temperature of the coil, 34.6 °C, is the highest among that of the coil, core, Al plate and coil base. The agreement between experimental results and the theoretical simulation results shows that the thermal field simulation can accurately predict the temperature of the magnetic coupler by reasonably setting the thermal power addition method.

INDEX TERMS Magnetic coupler, temperature characteristic, thermal circuit model, wireless power transfer system (WPT).

I. INTRODUCTION

With clean energy as the power source, electric vehicles (EVs) have the advantages of pollution-free, noiseless operation and low maintenance cost [1], [2]. Wired charging is a traditional way of energy supply for EVs that requires a cable connection between the charging station and EVs. Many technical problems, such as oxidation susceptibility and low universality or compatibility, are often associated. In the process of charging, due to metal contact, the living body will be injured in extreme weather conditions such as rain and snow [3]. Wireless power transmission (WPT) provides electrical isolation and reduces the cost, weight and volume of on-board charging [4]. Some

researchers have developed wireless charging systems for electric vehicles, thus solving many disadvantages of wired charging [5], [6]. In the related research, the temperature change of the magnetic coupler in the process of operation is often ignored [7]. In the WPT system, each component will produce losses [7], [8]. The loss of the magnetic coupler accounts for a large part of the total losses and eventually leads to a temperature rise [9]. Although the temperature rise of the magnetic coupler will not affect the power flow, the voltage gain and the power gain of the WPT system, it will threaten the stability of the WPT system [10], and affects the parameters of the ferrite material [11]. As with all electrical systems, significant thermal stresses in magnetic couplers can cause component failure, which is usually commonly irreversible and fatal. Especially in some applications, the maximum temperature is so high that it leads to the core burst.

The associate editor coordinating the review of this manuscript and approving it for publication was Dwarkadas Pralhaddas Kothari.

Therefore, it is essential to analyze the thermal characteristics of the magnetic coupler.

Many studies have focused on coupled simulation of magnetic and thermal fields. [12] and [13] present an analytical electromagnetic-thermal model. However, the results only suitable for a 2-D model. Besides, only eddy current loss is considered as the main heat source in [13]. Reference [14], [15] established a time-dependent multiphysics model for the design and analysis of wireless electric vehicle charging systems. COMSOL Multiphysics software is used for performing the finite element analysis based multi-physics simulations on a case study inductive electric vehicle wireless charging system. The results show that using the multi-physics model, the thermal behavior of the system can be effectively analyzed. However, the loss of each component can be calculated only when the frequency or output power changes. Reference [16] investigated the effect of the operation frequency of an inductive charging system on the heat generation and its impact on the overall system efficiency. Considering the influence of frequency and temperature on material properties, the finite element modeling software ANSYS workbench was used for analysis. To perform subsequent optimization faster, an order-reduced model is constructed in system-level simulation. Various tests show that the results of the reduced-order model agree well with those of the dynamically coupled-field solvers. However, although the heat loss of each component is discussed, the temperature distribution of each component is not given, and only the coil and shell temperature are measured.

Some research results on temperature characteristics and heating mechanism of magnetic couplers have been proposed. Many studies have been carried out on the loss of the components of the magnetic coupler [15], [17]–[19]. However, the temperature rise and temperature distribution caused by the loss have not been studied. Reference [7] proposed that temperature rise can be effectively improved by using coil materials and capacitors with strong temperature robustness and using heat sink in the WPT system. Furthermore, the research on the heating mechanism and temperature distribution of the magnetic coupler is very important for the further thermal optimization of the magnetic coupler. Based on a typical WPT system for pacemaker charging, [20] numerically solved the temperature distribution of the pacemaker and the surrounding area. However, the continuous working time of the charging system is short, and the thermal problem is not easy to expose. In [12], a thermal analysis of a buried double-D (DD) primary pad was proposed. An electromagnetic-thermal simulation was used to predict the steady-state temperature of the transmitter, but the loss of the aluminum shield plate, which affects the temperature distribution significantly, was not considered. The thermal simulation was used to discuss the thermal behavior of the couplers operating under load and a thermal equilibrium temperature measurement of each component was conducted in [22]. However, the relationship between the temperature of each component of the magnetic coupler has not been discussed,

which is the basis of more accurate thermal optimization. The thermal analysis of primary coils is also carried out in [10]. The change of temperature around the rectangle-shaped and the multi-thread primary coils is compared. However, the mechanism of temperature rise and temperature distribution are not further discussed. Reference [23] presented an experimental method to accurately measure power loss in magnetic couplers used in WPT systems. But only the temperature distribution of the whole magnetic coupler is given, and the temperature distribution characteristics of each component are missing. The temperature rise of the magnetic coupler of a 3.3 kW EV WPT system is studied [24]. Although the temperature distribution of each component is given, the coil loss is regarded as the main heat source. The eddy current loss of the aluminum shield plate and the loss of core are not considered. Similarly, [25] only considers coil heating.

Considering the issues of the current researches, two deficiencies can be found:

1) Thermal simulation is utilized to predict the temperature of the magnetic coupler. However, detailed and comprehensive theoretical calculation has not been carried out.

2) There is a lack of research on the temperature distribution of the magnetic coupler. Due to the incomplete heat source, it is hard to recognize the real temperature relationship of each component.

To supplement the above deficiencies, in this paper, the thermal characteristic of the magnetic coupler is studied. The thermal circuit model of the magnetic coupler is established, and its heat conduction and heat dissipation are analyzed. The temperature rise mechanism of each component of the magnetic coupler is studied. Then, the calculation results of the temperature of each component are simulated, which will be verified by the experiments finally.

II. MODELING OF MAGNETIC COUPLER AND THERMAL CIRCUIT MODEL

A. MODEL OF MAGNETIC COUPLER

The coil structure recommended by SAE J2954 [26] is selected to carry out simulation and experimental research. The coil design parameters are shown in Table 1. The transmitter is laid on the ground and has certain heat dissipation conditions. The receiver is a vehicle-mounted device, which has high requirements for thermal reliability, so this paper takes the receiver as the research object. The model and structure of WPT3 receiver are shown in Fig. 1. The materials and related parameters used for each component are shown in Table 2.

The air gap between different components is necessary, which is determined by the electrical performance of the coupler. The air gap between aluminum plate and core is 6 mm, and that between core and coil is 2 mm. From the aspect of thermal analysis, the properties of the materials between the air gaps have an important impact on the heat conduction in the receiver cavity. Therefore, in the actual production and simulation modeling, these parts are filled with appropriate materials as shown in Fig. 1.
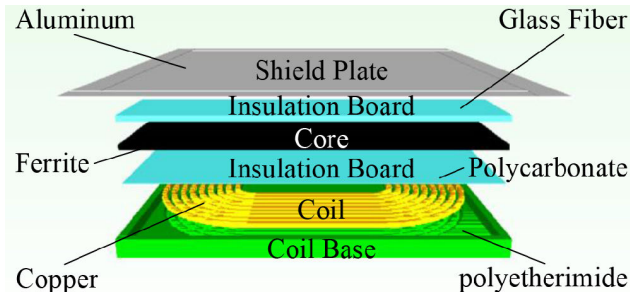
FIGURE 1. The structure of WPT3 magnetic coupler model.

TABLE 1. Coil design parameters.

Parameters	Transmitter coil	Receiver coil
Self-inductance	45.25 µH	38.77 µH
Internal resistance	60.5 mΩ	41.8 mΩ
Turns	8	10
Turn spacing	6.5 mm	
Mutual inductance	9.96 µH	
Coupling coefficient	0.11	
Air gap	100 mm	

TABLE 2. Relevant parameters of materials.

Component	Material	Thermal Conductivity (at 25 °C)	Emissivity (at 25 °C)
Coil	Copper	385.00 W/mK	0.80
Core	Ferrite	5.50 W/mK	0.74
Shield Plate	Aluminum 6061	180.00 W/mK	0.50
Coil Base	Polyetherimide	0.22 W/mK	0.93
Insulation	Polycarbonate	0.20 W/mK	0.93
Board	& Glass Fiber	1.09 W/mK	0.93

B. THERMAL RESISTANCE CIRCUIT OF MAGNETIC COUPLER

Due to the temperature difference, heat will be transferred within or between systems. In thermodynamic theory, Fourier's law describes the relationship between temperature difference and heat flux

$$\phi = \frac{kS\,\Delta T}{\delta} = \frac{\Delta T}{R_T} \tag{1}$$

where Φ is the heat flux, ΔT is the temperature difference, R_T is the thermal resistance, k is the thermal conductivity, S is the heat transfer area, and δ is the length of the heat transfer path.

In circuit theory, Ohm's law describes the relationship between voltage and current

$$I = \frac{U}{R_E} \tag{2}$$

where I is current, U is voltage, R_E is resistance.

Equation (1) and (2) show that the heat transfer is similar to the charge transfer in the circuit, so the process of heat transfer can be compared with the process of current flowing in the circuit. The concept of thermal resistance is introduced
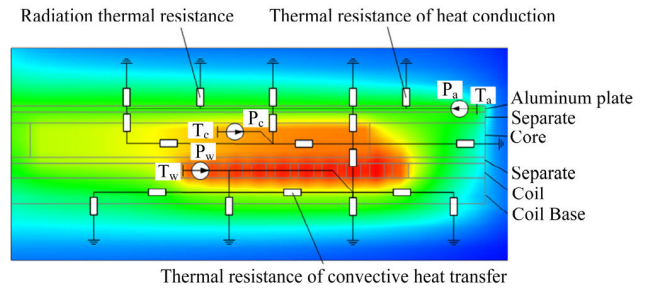

FIGURE 2. The thermal resistance model of the receiver.

to describe the heat resistance on the transfer path. In terms of expression, the concepts of resistance, voltage and current in the circuit field can be equivalent to thermal resistance, temperature and heat flow, respectively.

The thermal circuit model helps analyze the heat transfer situation and gives the temperature characteristics of each component from a qualitative perspective. Taking the cross-sectional side view of the receiver as the background, draw the thermal circuit model, as shown in Fig. 2. P_W, P_c, and P_a are heat sources, which represent the thermal power of the coil, core, and aluminum shield plate, namely the loss of the coil, core, and aluminum shield plate. T_W, T_C and T_A represent the temperature values of the coil, core, aluminum shield plate at the selected point, respectively. Heat conduction, heat convection and heat radiation are three basic forms of heat transfer. In the receiver cavity, the heat is mainly transferred by heat conduction, and the main thermal resistance is shown in Fig. 2. On the upper surface of the aluminum shield plate and the lower surface of the coil base, heat is transferred in the form of thermal radiation and natural convection. The corresponding radiant thermal resistance and convection heat resistance have been drawn.

A detailed discussion of the heating power will be given in section III. Here, only the qualitative analysis of the temperature conditions of the components of the magnetic coupler brought about by heat conduction will be conducted. The heating power of the coil is usually the largest, even accounting for more than half of the total loss of the magnetic coupler, so the coil usually has the highest temperature. The closer the core is to the coil, the smaller the thermal resistance and the closer the temperature to the coil. The wire reel is a non-metallic material, which does not cause any loss. Due to the close contact with the coil, its temperature rise comes from the heat conduction of the coil. The thermal resistance between the upper and lower surfaces is larger, so there will be a temperature difference between the upper and lower surfaces.

III. LOSS ANALYSIS OF MAGNETIC COUPLER
A. LOSS OF LITZ WIRE COIL
The temperature rise of the coil is mainly due to Litz wire coil losses, including the ohmic loss and the losses associated with skin and proximity effects.
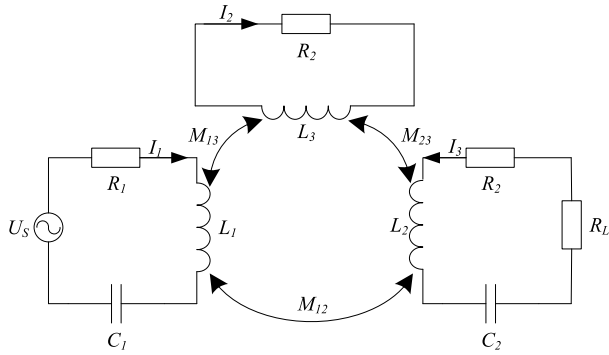
FIGURE 3. Equivalent circuit model of magnetic coupler.

The ohmic loss in the coil wires can be computed as

$$P_{ohmic} = \iiint_{V_w} j^2 \rho dV_w = I_w^2 R_w \tag{3}$$

where P_{ohmic} is the ohmic loss of the coil, ρ is resistivity, V_w is the volume of the coil, I_w is the current of the coil, R_w is the resistance of the entire wire [16].

The coil losses associated with skin and proximity effects can be approximated as

$$P_{skin\&prox} = (G_{skin} + G_{prox})i_{rms}^2 R_{DC} \tag{4}$$

where $P_{skin\&prox}$ is the coil losses associated with skin and proximity effects, G_{skin} is the loss factors that represent the skin effect, G_{prox} is the loss factors that represent the proximity effect, i_{rms} is the RMS current of the coil. R_{DC} is the DC resistance of the coil [14].

In summary, the losses of the coil can be calculated as

$$P_w = P_{ohmic} + P_{skin\&prox} \tag{5}$$

B. LOSS OF FERRITE CORE
The temperature rise of the ferrite core is mainly due to its loss. The loss density in the ferrite cores can be calculated using the Steinmetz equation as

$$P_c = k_s f^\alpha \hat{B}^\beta \tag{6}$$

where P_c is the core loss per unit volume, f is the operating frequency of excitation, $\hat{B}$ is the peak flux density, k_s, α and β are Steinmetz empirical constants [14], [27]. For different materials, the manufacturer will generally provide a set of corresponding constants. In general, $1 < \alpha < 3, 2 < \beta < 3$.

The total loss in the ferrite core can be calculated as

$$P_c = k_s f^\alpha \int_{V_c} \hat{B}^\beta dV_c \tag{7}$$

where V_c is the volume of the ferrite core.

C. LOSS OF ALUMINUM SHIELD PLATE
The equivalent circuit model is established to analyze the aluminum shield plate loss, as shown in Fig. 3. The shield plate

is equivalent to a circuit with resistance R_3 and inductance L_3 in series.

The matrix equation of the equivalent circuit is

$$\begin{bmatrix} \dot{U}_s \\ 0 \\ 0 \end{bmatrix} = \begin{bmatrix} Z_{11} & j\omega M_{12} & j\omega M_{13} \\ j\omega M_{12} & Z_{22} & j\omega M_{23} \\ j\omega M_{13} & j\omega M_{23} & Z_{33} \end{bmatrix} \begin{bmatrix} \dot{I}_1 \\ \dot{I}_2 \\ \dot{I}_3 \end{bmatrix} \tag{8}$$

Z_{11}, Z_{22} and Z_{33} are expressed as

$$Z_{11} = R_1 + j\frac{\omega L_1 - 1}{\omega C_1} \tag{9}$$

$$Z_{22} = R_2 + R_L + j\frac{\omega L_2 - 1}{\omega C_2} \tag{10}$$

$$Z_{33} = R_3 + j\omega L_3 \tag{11}$$

In order to simplify the analysis process, the mutual inductance between the aluminum shield plate and the primary coil M_{13} is ignored. Only the mutual inductance between the aluminum shield plate and the secondary coil M_{23} and the mutual inductance between the primary and secondary coils M_{12} is considered. Then the current of each part can be given as

$$\dot{I}_1 = (Z_{22}Z_{33} - Z_{23}^2)(Z_{11}Z_{22}Z_{33} - Z_{11}Z_{23}^2 - Z_{12}^2 Z_{13})\dot{U}_s \tag{12}$$

$$\dot{I}_2 = -Z_{12}Z_{33}(Z_{11}Z_{22}Z_{33} - Z_{11}Z_{23}^2 - Z_{12}^2 Z_{13})\dot{U}_s \tag{13}$$

$$\dot{I}_3 = -Z_{12}Z_{13}(Z_{11}Z_{22}Z_{33} - Z_{11}Z_{23}^2 - Z_{12}^2 Z_{13})\dot{U}_s \tag{14}$$

The loss of the aluminum shielding plate is calculated as

$$P_a = \left| \dot{I}_3 \right|^2 R_0 \tag{15}$$

R_0 in (15) considering skin effect can be calculated as

$$R_0 = \frac{\rho l_{eff}}{A_{eff}} \tag{16}$$

A_{eff} is the equivalent conductive cross-sectional area and l_{eff} is the equivalent conducting path distance [28].

D. LOSS RATIO OF EACH PART
The loss of each component of the magnetic coupler is dissipated in the form of heat energy and finally shows as temperature rise. A magnetic coupler model is established according to the parameters listed in Table 1. As shown in Fig. 4, the losses of each component of the magnetic coupler are calculated.

The loss of each component corresponds to the 6.6 kW power level of the WPT system. The loss of the coil accounts for 78.2 % of the total loss, which makes it have the highest temperature. The specific temperature distribution of each component will be discussed in section IV.
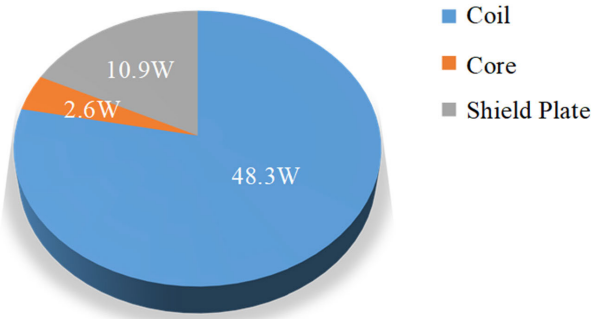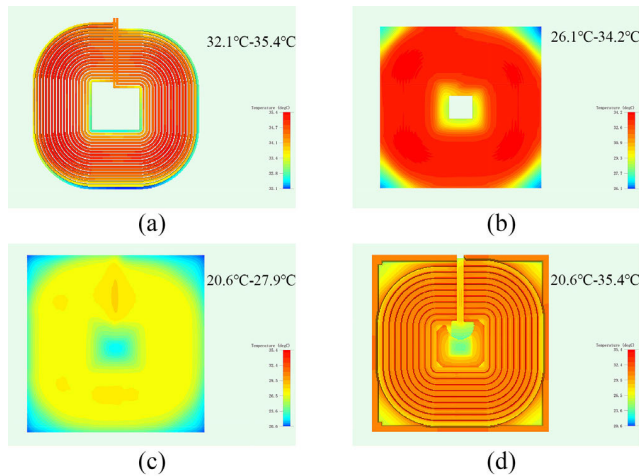
FIGURE 4. Loss of each component of magnetic coupler.

TABLE 3. Internal and external loss ratio of aluminum shield plate.

Outer ring width	Proportion of external loss	Proportion of internal loss
0 mm	0	100.0 %
1.0 mm	40.3 %	59.7 %
5.5 mm	51.6 %	48.4 %
10.0 mm	64.0 %	36.0 %
100.0 mm	98.8 %	1.2 %
162.5 mm	98.9 %	1.1 %

FIGURE 5. Thermal equilibrium temperature distribution of coil, core and coil base.

IV. SIMULATION OF TEMPERATURE DISTRIBUTION

The temperature distribution of the magnetic coupler is simulated based on the thermal power solved in Section III. The temperature distribution of each component is shown in Fig. 5.

Due to the use of Litz wire, the heating power of the coil is approximately uniformly distributed in the length direction of the wire, and it has been assumed that the contact between the coil and the core base is good when setting the characteristics. As shown in Fig. 5(a), the temperature of each turn in the radius direction of the coil rises and then decreases from inside to outside. This is because each turn of the coil is an independent heat source, the heat source located in the middle is hindered by the side heat source, the heat dissipation in the horizontal direction is restricted, and the heat sources located at the inner and outer edges have better heat dissipation conditions. So the middle coil has a larger temperature rise than the two sides.

The temperature distribution of the core is shown in Fig. 5(b). Comparing Fig. 5(a), it can be seen that the high-temperature area of the core reflects the shape of the coil, and the maximum temperature of the core is close to the maximum temperature of the coil, while the difference of the

lowest temperature is larger. This is because the coil is close to the core, the closer it is to the coil, the smaller the thermal resistance, and the closer the temperature of them, which is in line with the law of heat conduction. The coil base itself does not cause losses, and its temperature rise comes from the heat conduction of the coil. The temperature distribution of the coil base is shown in Fig. 5(c) and (d). The upper and lower surfaces of the coil base also have certain differences. The upper surface and the coil are bonded, so the temperature and the surface of the coil are basically the same. The thermal resistance between the upper and lower surfaces is larger, so the lower surface temperature is lower.

When the temperature distribution of the aluminum shield plate is simulated, the heating power is added in different ways, and the temperature range and temperature distribution of the aluminum shield plate are quite different. Therefore, it is necessary to study the actual loss distribution of the aluminum shield plate and make a reasonable thermal power distribution so as to improve the accuracy of the simulation. Due to the high-frequency skin effect of the aluminum shield plate, the loss decreases with the eddy current distribution from the edge to the inside. The magnetic simulation software is used to calculate the loss by region. The aluminum shield plate is divided into an outer ring and an inner aluminum shield plate, the outer ring width is set as a variable parameter, and multiple values are taken for simulation. Then divide the aluminum shield plate into upper and lower layers. Since the aluminum shield plate is only 2 mm thick, the thickness of each layer is set to 1 mm. Table 3 and Table 4 show the distribution of loss in each area under two conditions. From the data in the table, it can be seen that the loss of the aluminum shield plate is higher at the edge and accounts for a larger amount on the side near the core.

Considering comprehensively, the division of the aluminum shield plate and the way of adding thermal power are as follows: the aluminum shield plate is divided into upper and lower layers, each 1mm thick. The upper-layer heating power accounts for 19.5 %, and the lower-layer power accounts for 80.5 %. Then divide it into outer ring and inner aluminum shield plate, the outer ring width is 10 mm, the thermal power accounted for 64.0 %, and the internal accounted for 36.0 %. The temperature distribution of the aluminum shield plate is shown in Fig. 6.
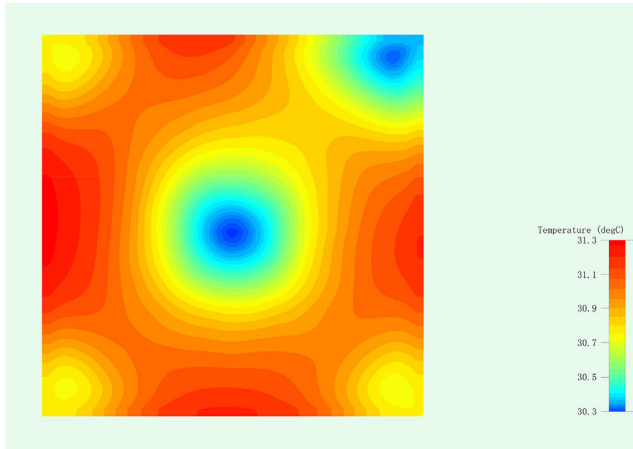
FIGURE 6. Thermal equilibrium temperature distribution of aluminum shield plate.

TABLE 4. Upper and lower loss ratio of aluminum shield plate.

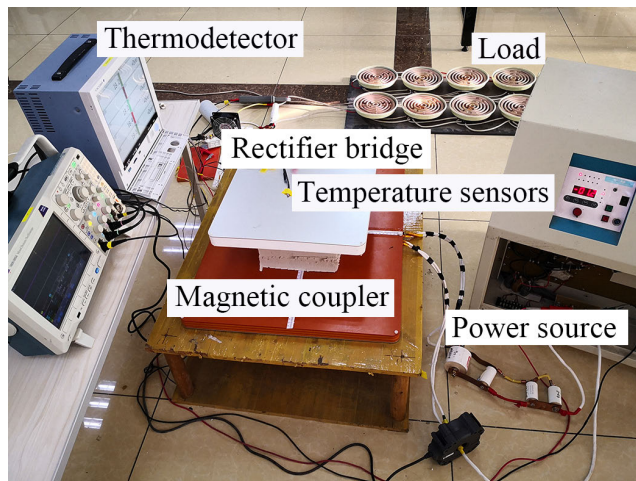| Lower thickness	Proportion of upper loss	Proportion of lower loss
1 mm	19.5%	80.5 %

FIGURE 7. Temperature measurement experiment setup.

V. EXPERIMENTAL VERIFICATION

A. EXPERIMENT SETUP

The temperature measurement prototype is built, as shown in Fig. 7. The system is consists of an inverter, compensation capacitors, magnetic coupler, rectifier and load. The system output power is 6.6 kW. The H-bridge inverter consists of four SiC MOSFETs (CMF20120D-ND) is utilized to provide 85kHz AC power for the system. The MOSFETs are driven by the high-speed gate driver IXDD614PI that is designed for high frequency and high power applications. The DSEI60-06A fast recovery diode is used to design the rectifier bridge. The diode is installed on the aluminum heat sink to cooperate with air cooling. The load is composed of five
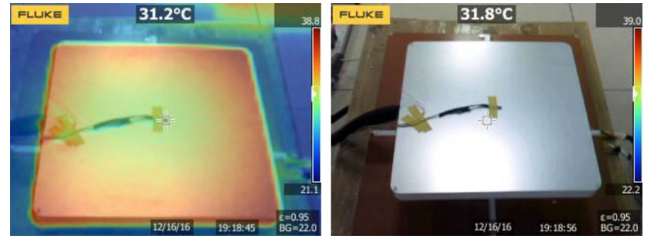

FIGURE 8. Thermo-vision image of the magnetic coupler.

electric furnace wires in series with a total resistance of 7 Ω, which can withstand a high temperature above 500 °C for a long time. platinum resistance and thermocouple sensors with smaller volumes are selected for temperature measurement.

The reference value of the air gap proposed in SAE J2954 (WPT3/Z2) is between 100 mm and 210 mm. The air gap of the experimental prototype is designed to be 100 mm, which can be flexibly adjusted within the standard range to adapt to the output power. The self-inductance and internal resistance of the magnetic coupler are measured by LCR meter in cases of alignment and misalignment. The self-inductance of the transmitter is 45.25 μH and the internal resistance is 60.5 mΩ. The self-inductance of the receiver is 38.77 μH and the internal resistance is 41.8 mΩ. The mutual inductance is 4.59 μH and the coupling coefficient is 0.11. The above parameters are within the range recommended by the standard, which ensures the feasibility of the experiment.

In order to obtain the temperature of each component of the magnetic coupler and make the experimental phenomenon more obvious, no passive or active cooler was applied to the magnetic coupler. In order to make the experimental prototype work normally and in a good working state, temperature measurement is carried out under the condition of coil alignment. In order to ensure that the temperature of the magnetic coupler is normal during the experiment, infrared thermal imager is used to monitor the temperature of magnetic coupler in real time during the experiment. Thermo-vision images taken by Fluke TiS20 thermal imager are shown in Fig. 8.

Fig. 9 shows the oscillogram waveforms of input and output electrical quantities measured at full-load operation by the current detector and voltage detector. The output voltage of the inverter and rectifier has been marked, i.e. primary voltage and secondary voltage of the magnetic coupler. And the primary current, secondary current and load current are also marked. The electrical parameters of each stage of power conversion are measured as shown in Table 5.

B. SELECTION OF TEMPERATURE MEASUREMENRT POINT
In this experiment, hot spots are selected for temperature measurement to find the most serious part of the temperature rise problem. The temperature measurement position of each component refers to the simulation results in Section IV.

As shown in Fig. 10, the yellow mark is the sensor position. Take the center position of the wire width as the coil, that is,

TABLE 5. Measured values of electrical parameters in each stage of power conversion.

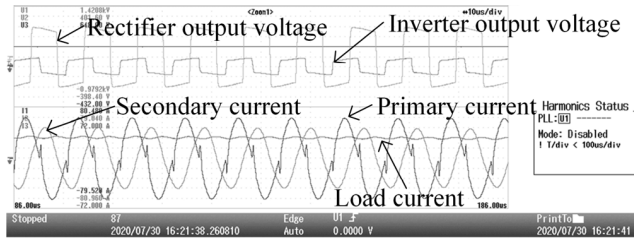| Parameters	Transmitter coil	Receiver coil	Load
Current	44.794 A	34.049 A	30.617 A
Voltage	0.1756 kV	0.2155 kV	0.2187 kV
Power	6.935 kW	6.772 kW	6.689 kW

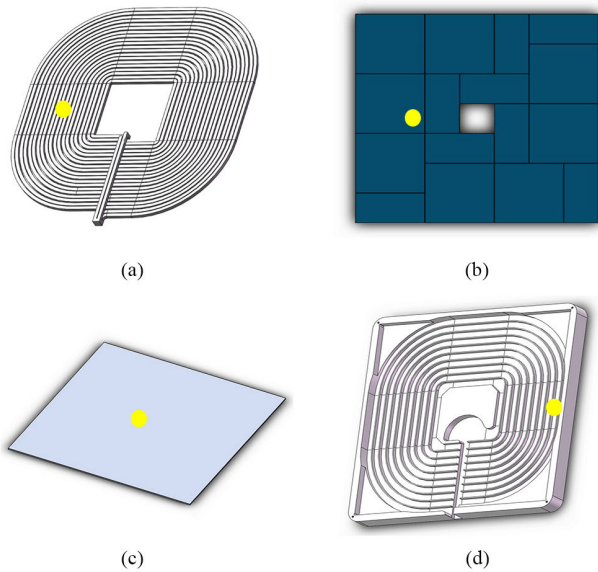**FIGURE 9.** Experimental system parameters and waveforms.

FIGURE 10. Temperature measurement position of each component of magnetic coupler.

the fifth turn from the inside to the outside; take the area near the center square hole as the core, about 50 mm from the edge of the square hole, close to the side of the aluminum shield plate; take the edge position as the coil base, corresponding to the coil the outermost turn; take the center of the outer surface as an aluminum shield plate.

C. RESULT ANALYSIS

The temperatures of the four channels were recorded by the Yokogawa GP10 thermometer. The temperature data of 30 minutes normal operation and 3 minutes after power-off are recorded, as shown in Fig. 11.

As shown in Fig. 11, the temperature curve is obviously shaken by magnetic field interference during power-on operation, and the temperature value changes suddenly after
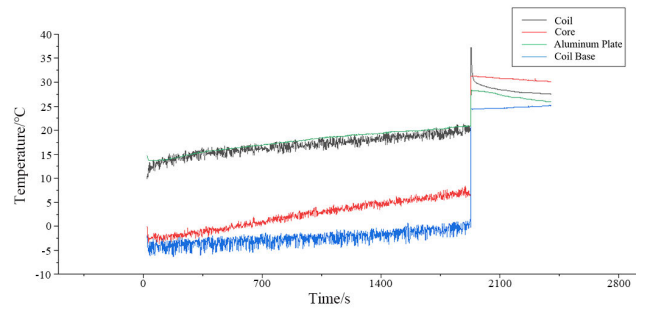

FIGURE 11. Temperature of each component.

TABLE 6. Experimental data and simulation data of each measuring point.

Position	Experimental	Simulation	Error
Coil	34.6 °C	34.4 °C	0.6 %
Core	31.2 °C	32.2 °C	3.2 %
Aluminum plate	28.3 °C	30.3 °C	6.6 %
Coil base	24.5 °C	23.3 °C	5.2 %

power-off. Sensors are placed in the magnetic field during the experiment. The metal probe of the sensor is heated by eddy current. When the magnetic field is removed, both the receiver and the sensor enter the natural cooling stage. Intercept the temperature curve that begins from powered off and maintain for 3 minutes, as shown in Fig. 12. The cooling process of the core, coil base and aluminum plate is always smooth. For the core and the aluminum shield plate, since the magnetic field at the sensor position has been shielded by the core or the aluminum shield plate, the eddy current heating is not obvious. The temperature measurement position of the coil base is far away from the coil, and the heating is not obvious. The temperature of the core, aluminum shield plate and coil base can be read directly.

The cooling curve of the coil can be divided into two stages. In the first stage, the temperature of the sensor heated by eddy current drops to the temperature of the measured point. Due to the small size of the sensor, the first stage of the process cools down quickly. When entering the second stage, the sensor can be regarded as a part of the measured position, and the temperature decreases slowly. The cooling rate changes abruptly at the critical point of the two stages, because the cooling objects of the two processes are different. The second derivative of the temperature curve of the coil is calculated and shown in Fig. 13.

As mentioned above, there is an obvious extreme point at 4 s, which is quite different from nearby values. Therefore, the corresponding temperature value at 4 s can be taken as the true temperature value of the measured point of the coil. Fig. 14 is the temperature data of each measuring point obtained by thermal field simulation. Experimental data, simulation data and their errors are shown in Table 6.

After the magnetic coupler works at 6.6 kW power level for 30 minutes, the coil temperature is the highest, followed by
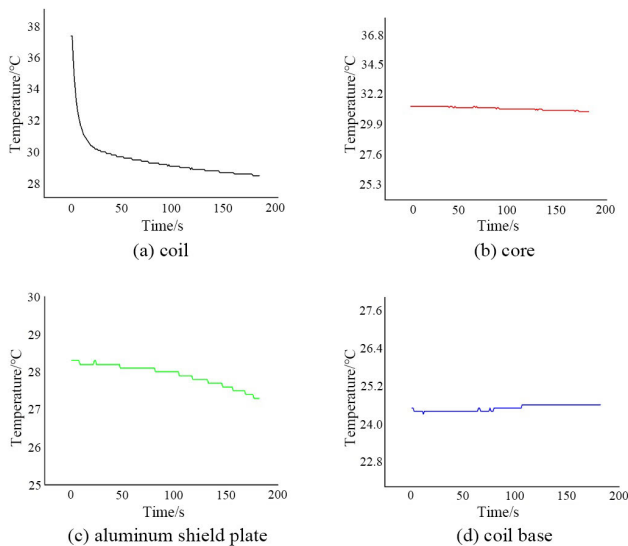
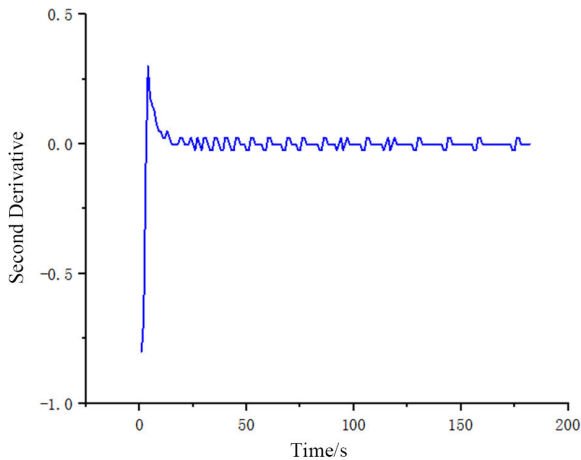**FIGURE 12. Temperature of each component of magnetic coupler.**

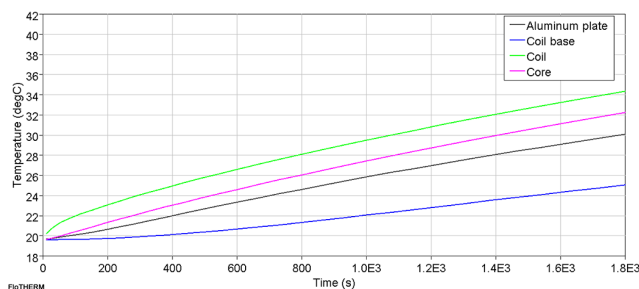**FIGURE 13. Second derivative curve of coil temperature.**

FIGURE 14. Simulation data of each measuring point.

the core and coil base, and the lowest temperature component is the aluminum plate. The experimental data is basically consistent with the simulation data. The above shows that it is feasible and accurate to use simulation to predict the temperature of the magnetic coupler.

VI. CONCLUSION

In this paper, a modeling and calculating method of the temperature distribution of a magnetic coupler is proposed.

Qualitative analysis shows that the temperature distribution of the components of the magnetic coupler is different. At the power level of 6.6 kW, coil loss, core loss and aluminum shield plate loss is 48.3 W, 2.6 W and 10.9 W, respectively, where the coil loss accounts for the most significant proportion and leads to the maximum temperature. After the 6.6 kW WPT prototype has been working for 30 minutes, the temperature of each component is consistent with the previous analysis, respectively. Specifically, the coil temperature is 34.6 °C, the core temperature is 31.2 °C, the aluminum plate temperature is 28.6 °C, and the coil base temperature is 24.5 °C. The experimental validation proves that the results of this paper can be applied in temperature prediction of the magnetic coupler in WPT system.

REFERENCES

[1] P. S. Subudhi and K. S, "Wireless power transfer topologies used for static and dynamic charging of EV battery: A review," *Int. J. Emerg. Electr. Power Syst.*, vol. 21, no. 1, pp. 365–399, Feb. 2020.

[2] E. Chemali, M. Preindl, P. Malysz, and A. Emadi, "Electrochemical and electrostatic energy storage and management systems for electric drive vehicles: State-of-the-Art review and future trends," *IEEE J. Emerg. Sel. Topics Power Electron.*, vol. 4, no. 3, pp. 1117–1134, Sep. 2016.

[3] Z. Bi, T. Kan, C. C. Mi, Y. Zhang, Z. Zhao, and G. A. Keoleian, "A review of wireless power transfer for electric vehicles: Prospects to enhance sustainable mobility," *Appl. Energy*, vol. 179, pp. 413–425, Oct. 2016.

[4] F. Musavi, M. Edington, and W. Eberle, "Wireless power transfer: A survey of EV battery charging technologies," in *Proc. IEEE Energy Convers. Congr. Exposit. (ECCE)*, Sep. 2012, pp. 1804–1810.

[5] G. A. Covic and J. T. Boys, "Modern trends in inductive power transfer for transportation applications," *IEEE J. Emerg. Sel. Topics Power Electron.*, vol. 1, no. 1, pp. 28–41, Mar. 2013.

[6] C. C. Mi, G. Buja, S. Y. Choi, and C. T. Rim, "Modern advances in wireless power transfer systems for roadway powered electric vehicles," *IEEE Trans. Ind. Electron.*, vol. 63, no. 10, pp. 6533–6545, Oct. 2016.

[7] K. Hwang, S. Chun, U. Yoon, M. Lee, and S. Ahn, "Thermal analysis for temperature robust wireless power transfer systems," in *Proc. IEEE Wireless Power Transf. (WPT)*, May 2013, pp. 52–55.

[8] C. Deqing, W. Lifang, L. Chenling, and G. Yanjie, "The power loss analysis for resonant wireless power transfer," in *Proc. IEEE Conf. Expo Transp. Electrific. Asia–Pacific (ITEC Asia–Pacific)*, Aug. 2014, pp. 1–4.

[9] D. Chae and Y. Kim, "Analysis for electrical and thermal hazard in kW-class wireless power transmission environment," in *Proc. IEEE PELS Workshop Emerg. Technol., Wireless Power Transf. (Wow)*, Jun. 2018, pp. 1–5.

[10] Z. Zhang, H. Pang, C. H. T. Lee, X. Xu, X. Wei, and J. Wang, "Comparative analysis and optimization of dynamic charging coils for roadway-powered electric vehicles," *IEEE Trans. Magn.*, vol. 53, no. 11, pp. 1–6, Nov. 2017.

[11] R. Bosshard, J. Muhlethaler, J. W. Kolar, and I. Stevanovic, "The η − α-Pareto front of inductive power transfer coils," in *Proc. 38th Annu. Conf. IEEE Ind. Electron. Soc. IECON*, Oct. 2012, pp. 4270–4277.

[12] T. Zhu, P. Feng, X. Li, F. Li, and Y. Rong, "The study of the effect of magnetic flux concentrator to the induction heating system using coupled electromagnetic-thermal simulation model," in *Proc. Int. Conf. Mech. Autom. Eng.*, Jul. 2013, pp. 123–127.

[13] D. Carstea, I. Carstea, and A. Carstea, "Numerical simulation of coupled magnetic and thermal fields in two-bars line," in *Proc. TELSIKS uth Int. Conf. Telecommun. ModernSatell., Cable Broadcast. Services*, Sep. 2005, pp. 311–314.

[14] M. Moghaddami and A. Sarwat, "Time-dependent multi-physics analysis of inductive power transfer systems," in *Proc. IEEE Transp. Electrific. Conf. Expo (ITEC)*, Jun. 2018, pp. 130–134.

[15] M. Moghaddami, A. Anzalchi, A. Moghadasi, and A. Sarwat, "Pareto optimization of circular power pads for contactless electric vehicle battery charger," in *Proc. IEEE Ind. Appl. Soc. Annu. Meeting*, Oct. 2016, pp. 1–6.

[16] M. Alsayegh, M. Saifo, M. Clemens, and B. Schmuelling, "Magnetic and thermal coupled field analysis of wireless charging systems for electric vehicles," *IEEE Trans. Magn.*, vol. 55, no. 6, pp. 1–4, Jun. 2019.

[17] S. Wang and D. G. Dorrell, "Loss analysis of circular wireless EV charging coupler," *IEEE Trans. Magn.*, vol. 50, no. 11, pp. 1–4, Nov. 2014.

[18] S. Wang and D. G. Dorrell, "Copper loss analysis of EV charging coupler," *IEEE Trans. Magn.*, vol. 51, no. 11, pp. 1–4, Nov. 2015.

[19] M. Moghaddami, A. Anzalchi, and A. I. Sarwat, "Finite element based design optimization of magnetic structures for roadway inductive power transfer systems," in *Proc. IEEE Transp. Electrific. Conf. Expo (ITEC)*, Jun. 2016, pp. 1–6.

[20] T. Campi, S. Cruciani, V. De Santis, and M. Feliziani, "EMF safety and thermal aspects in a pacemaker equipped with a wireless power transfer system working at low frequency," *IEEE Trans. Microw. Theory Techn.*, vol. 64, no. 2, pp. 375–382, Feb. 2016.

[21] S. Kim, M. Amirpour, G. Covic, and S. Bickerton, "Thermal characterisation of a double-D pad," in *Proc. IEEE PELS Workshop Emerg. Technol., Wireless Power Transf. (WoW)*, Jun. 2019, pp. 1–5.

[22] V. Kindl, R. Pechanek, M. Zavrel, T. Kavalir, and P. Turjanica, "Inductive coupling system for electric scooter wireless charging: Electromagnetic design and thermal analysis," *Electr. Eng.*, vol. 102, no. 1, pp. 3–12, Mar. 2020.

[23] G. Kalra, M. Pearce, S. Kim, D. J. Thrimawithana, and G. A. Covic, "A power loss measurement technique for inductive power transfer magnetic couplers," *IEEE J. Emerg. Sel. Topics Ind. Electron.*, early access, Aug. 6, 2020, doi: 10.1109/JESTIE.2020.3014823.

[24] K. Furiya, N. Omura, H. Nagano, K. Nishimura, A. Ueda, and S. Tokura, "Parallel-connected bilayer coil for a 3.3-kW electric vehicle wireless charging system," in *Proc. IEEE Wireless Power Transf. Conf. (WPTC)*, May 2017, pp. 1–4.

[25] J. Oiler, G. Anderson, V. Bana, A. Phipps, M. Kerber, and J. D. Rockway, "Thermal and biofouling effects on underwater wireless power transfer," in *Proc. IEEE Wireless Power Transf. Conf. (WPTC)*, May 2015, pp. 1–4.

[26] *Wireless Power Transfer for Light Duty Plugin Electric Vehicles and Alignment Methodology*. Accessed: Nov. 5, 2018. [Online]. Available: https://www.sae.org/standards/content/j2954_201711/

[27] R. W. Erickson and D. Maksimovic, *Fundamentals of Power Electronics*, 2nd ed. Boston, MA, USA: Springer, 200l.

[28] M. Mohammad, E. T. Wodajo, S. Choi, and M. E. Elbuluk, "Modeling and design of passive shield to limit EMF emission and to minimize shield loss in unipolar wireless charging system for EV," *IEEE Trans. Power Electron.*, vol. 34, no. 12, pp. 12235–12245, Dec. 2019.

FENG YUAN received the B.S., M.S., and Ph.D. degrees in instrument science and technology from the Harbin Institute of Technology (HIT), Harbin, China, in 1985, 1988, and 1995, respectively.

Since 2003, he has been a Ph.D. Supervisor with the School of Electrical Engineering and Automation, HIT. His research interests include measurement technology of precise geometric parameters and photoelectric detection technology.

XIAOHUA HUANG received the B.S. degree from the School of Electrical Engineering, Shandong University (SDU), Shandong, China, in 2002, and the Ph.D. degree in advanced technology of electrical engineering and energy from the Chinese Academy of Sciences (CAS), Beijing, China, in 2010.

She is currently a Senior Engineer with the China Electric Power Research Institute. Her research interest includes wireless power transfer.

YING SUN received the B.S. and M.S. degrees in instrument science and technology from the Harbin Institute of Technology (HIT), Harbin, China, in 2015 and 2017, respectively, where he is currently pursuing the Ph.D. degree in electrical engineering.

His research interests include wireless power transfer and foreign object detection.

CE LIANG was born in Fushun, Liaoning, China, in 1993. He received the B.S. and M.S. degrees from the School of Automation, Shenyang Aerospace University (SAU), Shenyang, China, in 2017 and 2020, respectively.

His research interests include wireless power transfer and detection technology.

JIN LI received the B.S. degree in electrical engineering from the Hebei University of Science and Technology (HEBUST), Shijiazhuang, China, in 1997.

He is currently a Deputy General Manager of the State Grid Hebei Electric Power Supply Company Ltd., Xiong'an New Area Power Supply Company. His research interests include low voltage DC applications and new energy.

GUANG YANG received the B.S. degree from the School of Electrical and Information Engineering, Anhui University of Technology (AHUT), Ma'anshan, China, in 2014, and the M.S. degree from the School of Electrical Engineering and Automation, Harbin Institute of Technology (HIT), Harbin, China, in 2017, where he is currently pursuing the Ph.D. degree.

His research interests include wireless charging technology for electric vehicles and other applications.

Mr. Yang was a recipient of the Best Paper Award from the 22nd International Conference on Electrical Machines and Systems (ICEMS2019).

KAI SONG (Senior Member, IEEE) received the B.S. and Ph.D. degrees from the School of Electrical Engineering and Automation, Harbin Institute of Technology (HIT), Harbin, China, in 2005 and 2011, respectively.

He joined the School of Electrical Engineering and Automation, HIT, as a Lecturer, in 2011. From 2014 to 2015, he was a Visiting Scholar in electrical engineering with The University of Tokyo, Japan. Since 2016, he has been the Deputy Director of the Institute of Wireless Power Transfer Technology, HIT. He is currently an Associate Professor with HIT. He has coauthored more than 60 peer-reviewed technical articles and authorized 30 invention patents in China. His current research interests include wireless power transfer, particularly in wireless charging systems for electric vehicles.

• • •